2026 IEEE International Conference on Robotics and Automation (ICRA 2026)
June 1-5, 2026. Vienna, Austria

Design and Validation of a Novel Quadruple-Disk CYcloidal Compact-cam Reducer for Robotic Applications: Q-CYC

Riccardo Bezzini[1], Giulia Bassani[1], Carlo Alberto Avizzano[1], and Alessandro Filippeschi[1]

***Abstract*— Reduction gearboxes play a key role in robotics actuation. Among the existing designs, cycloidal gears are gaining popularity for their efficiency, torque density, and robustness. The compact-cam architecture is a variant of the classical cycloidal drive that employs two rigidly coupled cycloidal disks to achieve high reduction ratios within a minimized radial profile. However, this design tends to suffer from low regularity, which can degrade performance in robotics applications. Building on the concept of the double disks with a phase offset to increase regularity, in this work, we present a novel Quadruple-disk CYcloidal Compact-cam (Q-CYC) reducer that applies the phase-offset principle to the compact-cam architecture. By incorporating two additional coupled disks, the proposed design enhances load distribution and motion regularity. Two open-source, 3D-printed prototypes (one implementing the conventional compact-cam transmission and one featuring the presented quadruple-disk architecture) are designed and experimentally evaluated. The analysis focuses on friction, gear play, backdriveability, and speed regularity, demonstrating that the quadruple-disk design offers significant improvements. Therefore, the results validate the effectiveness of the proposed approach in addressing known performance limitations of cycloidal compact-cam reducers, reducing gear play and improving both speed regularity and backdrivability.**

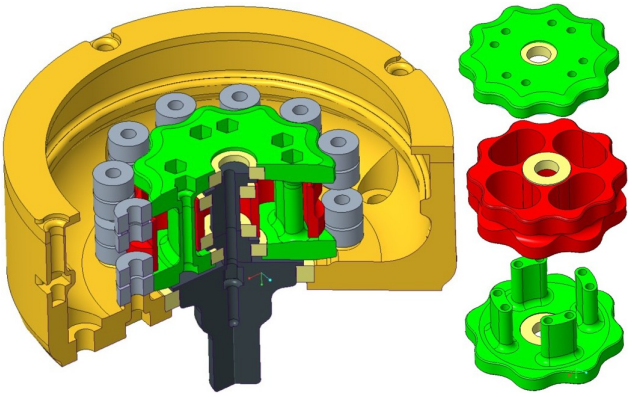

Fig. 1: Q-CYC design CAD views. On the left, an internal section view of the proposed prototype. On the right, an exploded view of the two compact-cam cycloidal disk pairs that assemble in the quadruple-disk architecture.

I. Introduction

Transmission systems and reduction gearboxes are critical components in robotics actuation, enabling the efficient conversion of motor power into controlled high-torque motion [1]. In applications where highly accurate dynamic performance is crucial, such as humanoid robotics and assistive exoskeletons, proper and effective reducers are essential to ensure precision, regularity, and efficiency [2], [3]. Among the various reduction architectures employed in robotics, such as planetary gearboxes [4] and harmonic drives [5], cycloidal gears emerge due to their resilience to impact, torsional stiffness, and efficiency [6].

These properties arise from their large force transmission areas, rolling contact dynamics, and simultaneous engagement of multiple teeth, which reduce localized stresses and allow for robust operation in dynamic environments [7], [8]. As such, cycloidal drives have found applications in articulated robots, humanoid platforms, and wearable devices where performance, reliability, and mechanical simplicity are critical [9], [10]. Multiple variants of cycloidal drives have been proposed in the literature, spanning from three-stage nested architectures [11], to double-roller drives [12], rotatable output-pin mechanism [13], and time-variant compound epicyclic-cycloidal reducers [14].

In contrast to the two-stage cycloidal design [15], [16], which still includes the presence of a carrier between the two stages, the compact-cam cycloidal architecture has been developed to further miniaturize gearboxes without sacrificing the reduction ratio [17], [18]. This configuration simplifies the classical mechanism by employing a single eccentric crankshaft and a pair of rigidly connected cycloidal disks, thus deleting the need for a carrier. This allows for the implementation of high reduction ratios in a compact radial form. However, despite their advantages, compact-cam reducers often exhibit reduced output smoothness, high vibration levels, and irregular torque profiles, especially at low speeds or under variable loading [19]. These drawbacks can significantly affect precision motion control and overall system stability. The experimental assessment of compact-cam cycloidal reducers conducted in previous work [20] confirmed its speed regularity issues, hence motivating the necessity of improving the compact-cam mechanism.

Traditional cycloidal reducers address the irregularity issues by employing two cycloidal disks rotated 180 degrees with respect to each other to minimize output torque ripple and enhance motion smoothness [21]. Moreover, the two

The purchase of the materials used in this work and part of the personnel costs were supported by the BRIEF "Biorobotics Research and Innovation Engineering Facilities" project (code IR0000036) funded under the National Recovery and Resilience Plan (NRRP), Mission 4 Component 2 Investment 3.1 of the Italian Ministry of University and Research funded by the European Union – NextGenerationEU. Part of the activities and the personnel of this work were supported by the Department of Excellence in Robotics and Artificial Intelligence, funded by the Ministry of Research and University (DM 230/2022).

[1] All the authors are with the Institute of Mechanical Intelligence and with the Department of Excellence in Robotics and AI, Scuola Superiore Sant'Anna, 56127, Pisa, Italy

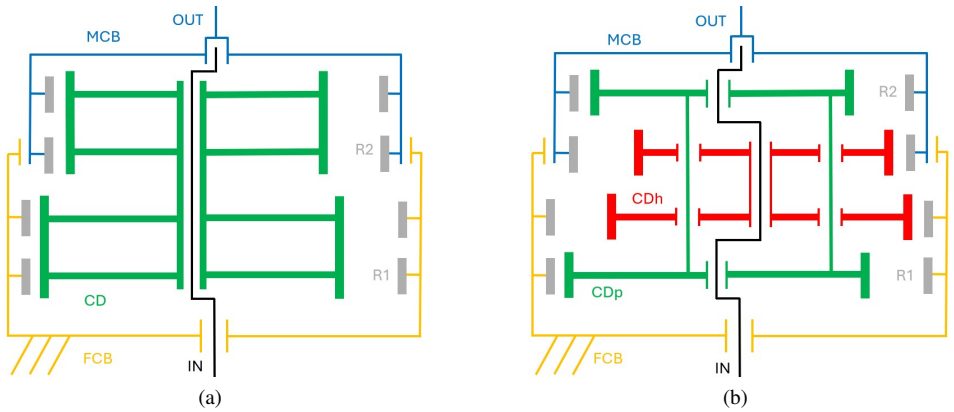

Fig. 2: Schematic illustrations of the classic cycloidal compact-cam layout (a) and the proposed quadruple-disk variant (b). The acronyms reference the same-color parts: IN is the input shaft (black, with eccentric sections), FCB represents the fixed cycloidal base (yellow), which is connected to the rollers (R, grey). R1 (first stage rollers) attaches to the fixed base; R2 (second stage rollers) attaches to the moving cycloidal base MCB, which is also the reducer's output (OUT). CD stands for the compact-cam cycloidal disk. In the quadruple-disk variant, CDp and CDh refer to two compact-cam pairs: CDp has pins, CDh has holes. Both disks are connected to the same shaft, but on different eccentric cams.

disks are assembled on oppositely eccentric cams of the input shaft [22]. These features enable a more uniform distribution of dynamic loads during operation, aiming to cancel out vibrational forces generated by eccentric rotation [23].

To address the limitations of the compact-cam architecture, this work introduces a novel Quadruple-Disk CYcloidal Compact-cam design (Q-CYC), employing the phase-offset principle through the incorporation of two additional disks (rigidly connected into a supplementary compact-cam disk) in the mechanism. Thus, the resulting architecture includes four cycloidal disks arranged in two phase-offset pairs of compact cams, as shown in Figure 1, mounted on oppositely eccentric cams of the same shaft. The goal is to enhance motion smoothness through distributed load transmission and increased contact frequency. To validate the proposed concept, two prototypes (implementing the conventional compact-cam design and the proposed quadruple-disk enhancement) have been designed and tested. Experimental investigations of the two 3D-printed prototypes include measurements of gear play, friction, angular velocity regularity, and output smoothness under different loading conditions. These experiments provide empirical evidence of the quadruple-disk approach's effectiveness and offer practical insights into its potential applications in robotics.

The novelty of this work lies in the extension of phase-offset principles to the compact-cam structure through the geometric definition of a novel quadruple-disk design. The main contributions of this paper are:

- The proposition and geometric definition of a cycloidal quadruple-disk gearbox architecture that addresses the limitations of compact-cam cycloidal reducers. An executable file for the design of custom quadruple disk cycloidal reducers is available at [24].
- The design of two 3D-printable cycloidal reducers, one conventional compact-cam and one implementing the proposed quadruple-disk architecture. The CAD models and BOMs are available at [24].
- An experimental evaluation that highlights the improvements offered by the Q-CYC design.

II. MATERIALS AND METHOD

A. Proposed Q-CYC Design

The novel quadruple disk (or double compact-cam) cycloidal design applies the dual 180-degree phase disk principle to the compact-cam cycloidal architecture. This arrangement aims to reduce the gear play and stabilize the output motion, both in free and loaded conditions, by guaranteeing more regular contacts between the rollers and the cycloidal disks through an additional double compact-cam disk (CCD).

In this architecture, the first CCD is mounted on an eccentric shaft as in the traditional system. However, to balance internal contact forces and improve motion transmission, the Q-CYC design incorporates an additional 180-phased CCD, composed of two rigidly connected disks mounted in phase opposition to the first compact-cam components. Besides being composed of joined differently oriented cycloidal disks, the additional CCD is assembled on an eccentric shaft cam that is opposed to the one on which the first compact disk is mounted, as can be seen in Figure 2.

The problem with applying the concept of the 180 phase disk to the compact cam architecture lies in the fact that, in this case, the additional disks (the green ones in Figures 1, 2b, 4c, and 4d) need to be attached, and the only way to implement such a solution is by including a connection that runs through the original CCD (the red one). As can be noted from the schematic sketch in Figure 2, in order to combine the additional two disks in a compact-cam element, a pinned connection is proposed between the additional disks, thus implying the presence of holes in the first compact-cam disk.

Pins and holes are critical for designing a couple of compact-cam disks that do not interfere with each other. In the following, the geometric conditions are presented to allow a proper implementation of the Q-CYC design, referring to Figure 3.

Given a cycloidal profile (see [25]), which is defined based on the number of rollers (N_r), their diameter (D_r), the diameter of the circumference which they are placed on (D_{pr}), and the eccentricity (E), we can define a circumference of diameter D_M that corresponds to the biggest circle contained in the disk profile that does not intersect it:

$$D_M = D_{pr} - D_r - 2 \cdot E. \tag{1}$$

Then, considering the central hole of diameter D_H for the shaft bearing housing, the pins and holes should be defined so that they are restrained to be contained between D_M and D_H, thus not interfering with each other's eccentric motion or obstructing the cycloidal profiles.

Another geometric constraint of the Q-CYC architecture is the relation between the connective pins and holes. Since they are connected to two oppositely eccentric cams of the input shaft, their centers are going to be constantly apart by $\pm 2 \cdot E$, as shown in Figure 3a. Thus, for the pins not to interfere with the holed disk, it must be ensured that:

$$D_{ch} = D_{cp} + 4 \cdot E, \tag{2}$$

where D_{ch} and D_{cp} are respectively the connective holes and pins' diameters. Thus, to sum up, the following conditions must be respected while designing a Q-CYC reducer:

$$D_{ph} + D_p + 4 \cdot E < D_M \tag{3}$$

$$D_{ph} - D_p - 4 \cdot E > D_H \tag{4}$$

where D_{ph} represents the pin-holes pitch circle, D_H is the disk's central hole, and D_M is the biggest circle contained in the disk profile that does not intersect it.

B. Geometric Design Tool

To ease and encourage the exploration and analysis of the proposed architecture, we provide an executable tool and its source code at [24] for the development of a custom Q-CYC reducer. Starting from the user's definition of the desired reduction ratio and maximum radial encumbrance, the proposed instrument presents all the possible combinations of N_{r1} and N_{r2} to obtain the target *i* (see equation 5). Once the number of rollers for the two stages is defined, the remaining parameters (E, D_{pr1}, D_{pr2}) for the cycloidal profile delineation are requested. At this point, a compact-cam geometry is already arranged. The next steps concern the definition of the connective pin-holes system, that is to say D_H, D_p, and D_{ph}. After the geometric definition of each variable, the resulting cycloidal profiles, rollers, holes, and pins are displayed through some sketches, to let the user check their choices and optionally change some of the parameters. Once all the selected variables are confirmed, two separate figures show the resulting view of the two sets of cycloidal disks, in a format similar to the one presented in Figure 3b.

C. 3D-Printed Prototypes

To evaluate the advantages of the presented design, two 3D-printed prototypes (whose CAD models and BOMs are available at [24]) have been developed. The first reducer is a classical compact-cam reducer (referred to as CC), while the second (QD) implements the novel Q-CYC design.

1) Design parameters: Given the Compact-cam ratio:

$$i = \frac{n_1 \, N_{r2}}{n_1 \, N_{r2} - n_2 \, N_{r1}}, \tag{5}$$

n_i denotes the number of disk lobes at the i^{th} stage and N_{ri} represents the number of rollers at the i^{th} stage. For designing the presented prototypes, we employed cycloidal profiles such that $n_i = Nr_i - 1$. In accordance with the previously presented geometric constraints, the same parameters (see Table I) have been used to design the two gearboxes, thus allowing for a fair comparison.

As shown in Figures 4c and 4d, the conjunctive pins were coupled in four pairs to improve their printability and rigidity, generalizing the conditions presented in the equations (1–4).

TABLE I: Prototypes geometric parameters

Symbol	Value	Description
i	-44	Reduction Ratio
D_{pr1}	45 mm	Rollers Pitch Diameter (Stage 1)
N_{r1}	9	Number of rollers (Stage 1)
D_{pr2}	45 mm	Rollers Pitch Diameter (Stage 2)
N_{r2}	11	Number of rollers (Stage 2)
D_r	8 mm	Roller Diameter
E	1.2 mm	Eccentricity
N_{ph}	8	Number of connection Pins-Holes
D_{cp}	3.7 mm	Connection Pin Diameter
D_{cp}	8.5 mm	Connection Holes Diameter
D_{ph}	22.8 mm	Connection Pin-Holes Pitch Diameter

2) Materials and Components: To fabricate the prototypes displayed in Figure 4, PLA was selected for its low cost and adequate mechanical performance [26]. The manufacturing process involved the Ultimaker S7 printer, slicing via Ultimaker Cura. Not additively manufactured components included bearings, screws, and nuts.

D. Experimental Assessment

1) Experimental Setup: The setup employed for the reducers' evaluation is composed of a brushless motor (EC 90 flat, 360 W, ϕ90, Maxon) with an integrated 2-channel encoder (MILE 512–6400 CPT, Maxon). The reducer's output is coupled to the incremental magnetic encoder (H2 Series, Phoenix America). These components are fixed to a set of beams through a support structure. The motor-encoder assembly is controlled by the driver (STEVAL-SPIN3201, STMicroelectronics). Two load cells (CZL635, Phidgets Inc.), which can be placed at the end of the output arm, are connected, together with the magnetic encoder, to the STM32 Nucleo-144 board (NUCLEO-F767ZI). Both boards are connected to the central unit (Intel NUC 11 Pro, i7-1165G7) running Windows 11 and Simulink (MATLAB,

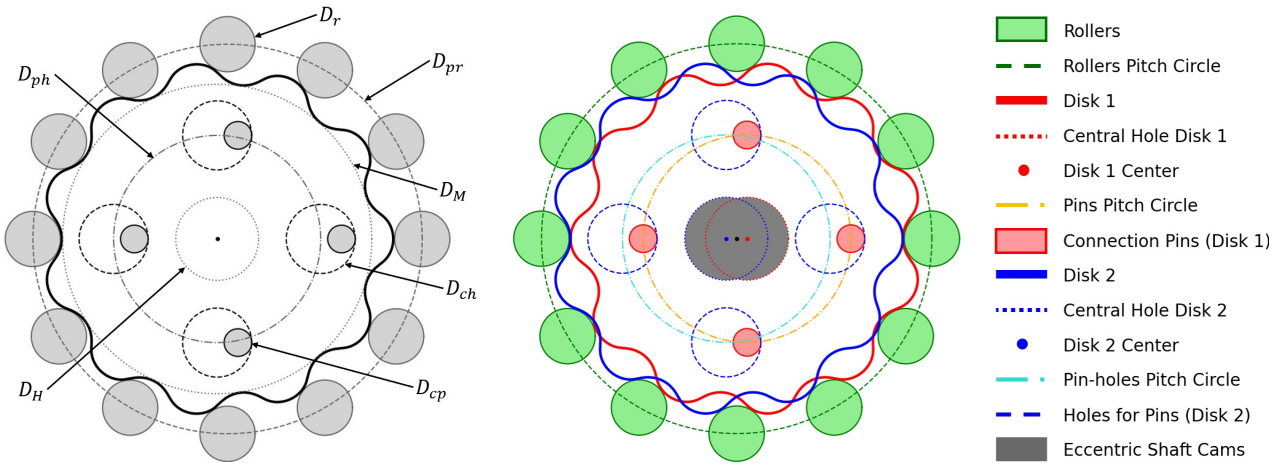

(a) (b)

Fig. 3: Illustrations of the disk-pin-holes set. (a) Representation of a cycloidal disk, with the connection pins and holes required by the Q-CYC design, engaging a set of rollers. (b) A drawing representing two overlapping 180-phased cycloidal disks that engage the same set of rollers but belong to two different compact-cam pairs of a Q-CYC reducer. The blue disk (2) includes the holes that let the connective pins (belonging to the red disk (1)) pass through and attach the displayed first-stage disk to the successive one (the second pair of disks is omitted, not to overload the figure).

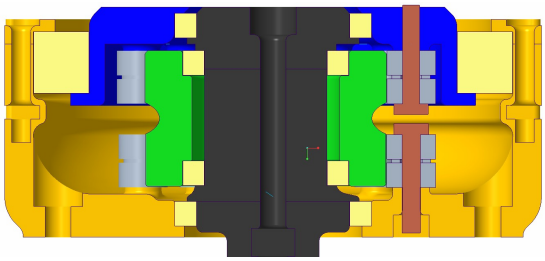

(a) Traditional Compact-cam Cycloidal prototype section view.

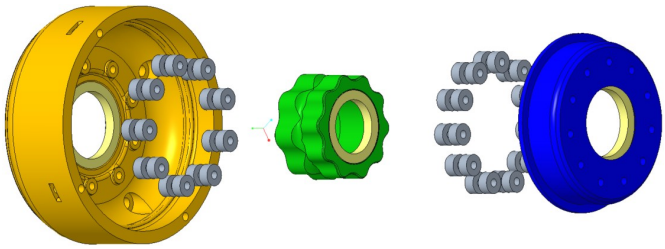

(b) Traditional Compact-cam Cycloidal prototype exploded view.

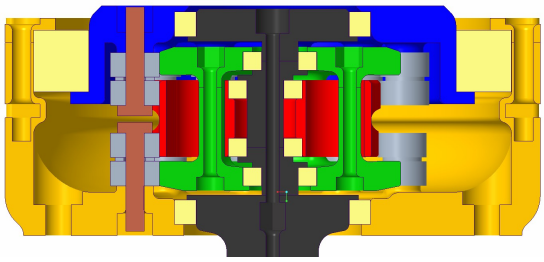

(c) Quadruple-Disk Cycloidal prototype section view.

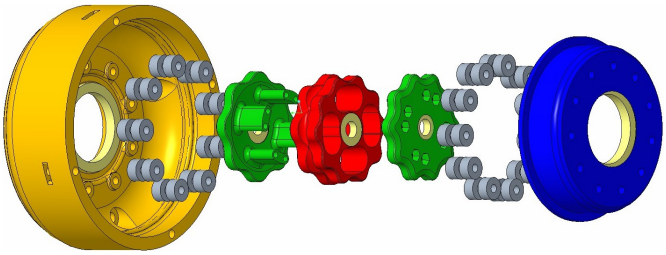

(d) Quadruple-Disk Cycloidal prototype exploded view.

Fig. 4: CAD illustrations of the proposed prototypes. The images (a) and (b) represent different views of the classic compact-cam prototype, while (c) and (d) depict the novel Q-CYC device. The employed colors respect the standard of Figure 2.

Mathworks Inc.), where a Kalman filter estimates the motor speed, and a PID controller has been designed for regulating the motor's speed. Figure 5 presents two photos of the experimental setup, highlighting the main components. The employed load cells are assembled in place of the load displayed in Figure 7b for some of the performed tests.

2) Experimental Metrics and Protocols:

a) Gear Play: Gear play is the reducer's output range of motion (locked-input condition) observed without resisting torques from the actuator. Lower gear play leads to more precise motion. It was estimated by measuring the maximum output motion without moving the motor axis, trying to manually move the reducer's output without applying significant torque to prevent joint stiffness from influencing the measured output motion. The test, consisting of attempting to move the output link while keeping the motor fixed, was conducted at $2i$ input positions evenly spaced by 180° motor rotations, allowing the gear play to be characterized over a complete revolution of the reducer's output. This analysis was performed three times for each reducer.

b) Backdrive Torque: The torque required at the reducer's output to initiate the motor's motion. The setup used to assess back-drivability employs both the arm and load cells, positioned at the end of the arm in place of the load shown in Figure 7b. The motor was aligned so that the output arm was horizontal, establishing a reference for correctly considering the torque from the arm and load weight, which depends on angular position. Increasing forces were manually applied to the load cells until motor motion was detected. The test was repeated at least five times in three separate sessions. Backdrive torque was then estimated by detecting the motor displacement (identified using a 0.18° threshold, twice the encoder resolution) and evaluating the corresponding enforced torque. The considered torque included the manually applied forces, the weight of the arm and load cells, and was corrected according to the output angle.

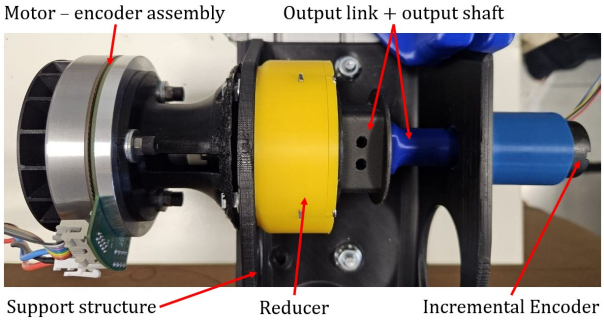

(a) Upper view of the experimental setup.

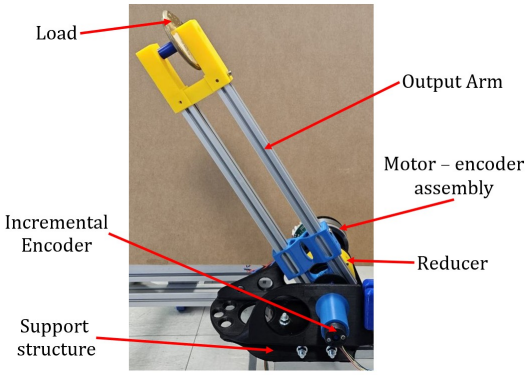

(b) Frontal view of the experimental setup.

Fig. 5: Experimental apparatus. Figure (a) represents a focus on the motor-reducer-encoder assembly, while (b) shows a frontal view of the setup, including the loaded output arm.

c) Friction: The required motor torque to overcome the static and viscous resisting forces. Friction was estimated by imposing slowly ramping motor speed references in the range of ±150 rad/s, following the method described in [23]. Each ramp signal was tracked by the motor three times, repeating the experiment thrice for each reducer. Motor's speed and current (torque) were employed to fit the friction model:

$$\tau_{fr} = \begin{cases} M_c^+ + d_v^+ \, \omega_m & \text{if } \omega_m \geq 0 \\ -M_c^- + d_v^- \, \omega_m & \text{if } \omega_m \leq 0 \end{cases} \tag{6}$$

where τ_{fr} denotes the friction torque, M_c denotes the static Coulomb friction component, d_v denotes the dynamic viscous factor, and ω_m denotes the motor velocity. Figure 6 displays the torque and speed data from one experiment for each reducer and the respective fitted model.

d) Speed Regularity: The relative deviation between the actual reducer's output speed and its expected value. It assesses the actuator's ability to maintain a definite speed. Both loaded and free-running conditions were considered. To assess the unloaded speed regularity (R_{uCC} and R_{uQD}), a PID controller was implemented to regulate the motor speed in response to a sequence of step references ranging from 0 rad/s to ±100 rad/s, with 20 rad/s increments (see Figure 7a). The same test was repeated three times with both positive and negative velocities.

To evaluate the reducers' regularity under different loads (R_{lCC} and R_{lQD}), an arm was connected to the output link. Considering the presence of the output arm, some position constraints were imposed on the reducers' output motion. Then, a sequence of ±20 rad/s speed steps (see Fgiure 7b) is given as reference. Given the reduced range of motion, a higher velocity step would have been too short to evaluate regularity. Three different loading conditions have been employed: L_0= 0.293 g, L_1= 0.594 g, and L_2= 0.896 g, presented as single loads put at the end of the lever arm (0.44 m). It should be noted that these values include both the output link weight and the additional loads.

Regularity is computed according to:

$$R = 100\left(1 - \frac{\Delta\omega_r}{i\,\omega_m}\right), \tag{7}$$

where R denotes the regularity (expressed as a percentage value), ω_r denotes the reducer's speed, i denotes the transmission ratio, and ω_m denotes the motor's velocity.

III. RESULTS AND DISCUSSION

The numerical results from the prototypes' experimental characterization are presented in Tables (II–V).

The introduction of the quadruple-disk architecture brought a significant improvement in gear play, reducing the mean output free motion from 0.361° to 0.056°. The QD prototype not only achieved an 85% improvement on the CC device, but also displayed a notably better gear play with respect to previous works on 3D-printed cycloidal reducers [20], [21], [23].

Regarding the friction resisting torques, as reported in Tables II and V, the QD static component resulted slightly higher than the one identified on the compact-cam device. In contrast, the viscous component of the identified friction model for the Q-CYC device displayed a reduction of ∼ 28% relative to the CC prototype (0.16–0.13 $mNms/rad$, compared to CC 0.21–0.19 $mNms/rad$), as confirmed by the graphs presented in Figure 6. This should be due in part to the presence of larger bearings between the shaft and disk in the compact-cam gearbox (as illustrated in Figure 4).

The much uniform load and contact distribution between rollers and disks (guaranteed by the Q-CYC architecture)

TABLE II: Prototypes friction models.

	Coulomb [mNm]		Viscous [mNms/rad]	
	M_c^+	M_c^-	d_v^+	d_v^-
CC	**44.42 ± 2.39**	**49.05 ± 2.89**	0.21 ± 0.04	0.19 ± 0.04
QD	48.65 ± 2.73	50.82 ± 1.12	**0.16 ± 0.02**	**0.13 ± 0.01**

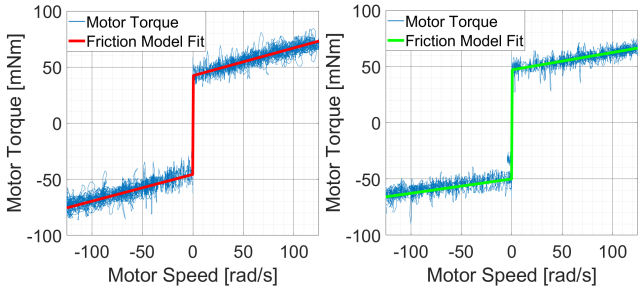

(a) CC prototype friction model. (b) QD prototype friction model.

Fig. 6: Example of friction test results (motor torque over motor speed) for the CC (a) and QD (a) prototypes.

contributed to a substantial regularity enhancement, confirming better transmission stability and reducing the speed oscillations, with an increase of $\sim 6\%$ and $\sim 10\%$ respectively in unloaded and loaded speed regularity (see Tables (III–IV).

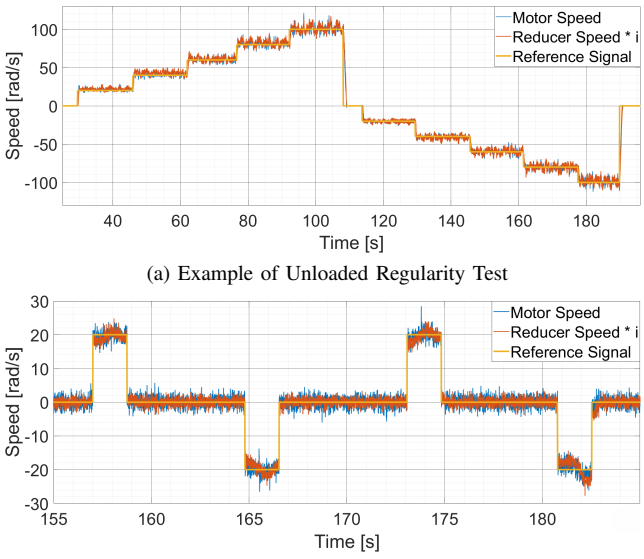

(a) Example of Unloaded Regularity Test

(b) Example of Loaded Regularity Test

Fig. 7: Examples of free (a) and loaded (b) regularity tests.

TABLE III: Prototypes Unloaded Regularity.

$\omega_m[rad/s]$	20	40	60	80	100
R_{uCC} [%]	86.55	90.25	90.98	91.07	91.02
R_{uQD} [%]	**95.29**	**95.62**	**95.46**	**95.49**	**95.44**

This improvement also affects the gearbox acoustic noise: the QD prototype presented significantly lower sound emissions, as confirmed by the video attachment registered during

TABLE IV: Prototypes Loaded Regularity.

Load	L_0	L_1	L_2
R_{lCC} [%]	84.43	84.71	83.96
R_{lQD} [%]	**94.56**	**93.37**	**94.29**

a sequence of speed steps ranging from 20 to 100 rad/s.

An important aspect of the experimental results concerns the backdriveability of the two prototypes. The CC reducer was not backdrivable under the tested torque levels (up to 20 Nm). In contrast, the QD device exhibited backdriveability with required torques of ~ 2.45 Nm, resulting well within the range of interest for safe human–robot interaction and compliant robotics actuation.

The underlying mechanical reasons for this difference require further investigation. However, a plausible explanation lies in the kinematic configuration of the QD design. The introduction of the dual compact-cam stages (assembled on oppositely eccentric cams of the input shaft) certainly promotes more uniform contact conditions between the rollers and the cycloidal disks. Since the ability to initiate backdriving depends on the relative positions of the rollers and disks in both the transmission stages, this improved uniformity likely ensures that, at any given angular position, the distributed interaction contacts allow the transmission of forces sufficient to trigger motion. These results suggest that the QD architecture is inherently favorable for achieving backdriveability compared to the CC, opening promising perspectives for applications where transparency and force control are required.

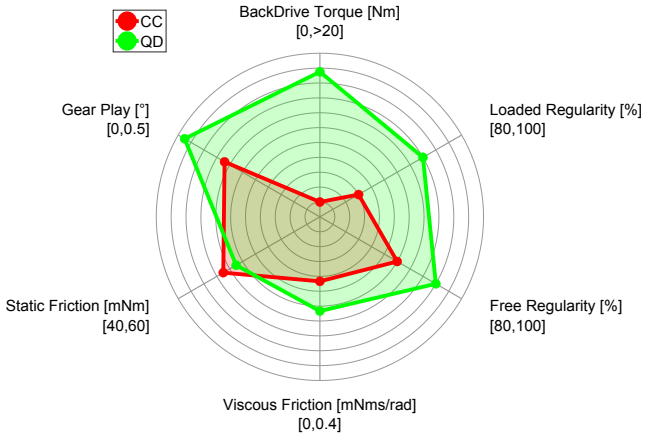

Fig. 8: Spider plots for synthesizing the prototypes' performances regarding the considered metrics, allowing a straightforward and comprehensive comparison of the presented devices. The measurement units are specified together with the minimum and maximum values displayed in the plot. The best value for each metric, e.g., backdrive torque equal to zero or 100% regularity, is set on the outer circle. Thus, the larger the area inside the plot, the better the gearbox.

As reported in Table V and summarized by the spider plots presented in Figure 8, the Q-CYC architecture proved

notable advantages regarding almost all the analyzed metrics. The QD prototype demonstrates superior performance in terms of gear play, motion regularity, backdrive torque, and viscous friction reduction, which are critical for high-precision robotic applications. The CC, while simpler in design, suffers from higher gear play and particularly reduced regularity under load. These results highlight the trade-offs between mechanical simplicity and dynamic performance: the QD architecture effectively minimizes non-idealities in the compact-cam cycloidal transmission.

TABLE V: Prototypes performance overview.

	CC	QD
Gear play [°]	0.361 ± 0.116	$\mathbf{0.056 \pm 0.021}$
Coulomb friction [mNm]	$\mathbf{46.73 \pm 3.52}$	49.74 ± 1.54
Viscous friction [mNms/rad]	0.200 ± 0.029	$\mathbf{0.145 \pm 0.011}$
Backdrive torque [Nm]	> 20	$\mathbf{2.452 \pm 0.081}$
Free regularity [%]	89.97 ± 1.12	$\mathbf{95.78 \pm 0.99}$
Loaded regularity [%]	84.37 ± 0.38	$\mathbf{94.07 \pm 0.62}$

IV. CONCLUSIONS

This paper proposes a novel Quadruple Disk Compact-Cam architecture, designed to address the limitations of gear play and speed regularity commonly observed in classic compact-cam reducers. Building on the phase-offset disk concept, this design introduces an additional pair of coupled disks that are assembled on a cam of the shaft with an eccentricity equal and opposite to that of the first compact-cam disk. An experimental evaluation has been carried out on two 3D-printed prototypes to validate the proposed architecture with respect to the compact-cam mechanism in terms of standard reducer performance metrics, including friction, gear play, and regularity. The results demonstrate that the proposed Q-CYC configuration provides significant improvements in regularity, gear play, and backdriveability compared to the conventional compact-cam design.

Future work will include a comprehensive theoretical study to investigate the impact of the main design parameters on the proposed architecture, to optimize its design based on operational conditions.

REFERENCES

[1] P. L. García, S. Crispel, E. Saerens, T. Verstraten, and D. Lefeber, "Compact gearboxes for modern robotics: A review," *Frontiers in Robotics and AI*, vol. 7, p. 103, 2020.

[2] L. Xu and Y. Wu, "Investigation of the dynamic transmission accuracy of an industrial robot joint rv reducer under variable situations," *Multibody System Dynamics*, pp. 1–38, 2025.

[3] W. Shin, B. Ahn, and S. Kwon, "A low backlash and highly efficient gearbox for robot actuator," in *2024 IEEE International Conference on Advanced Intelligent Mechatronics (AIM)*, pp. 224–229, IEEE, 2024.

[4] S. Landler, M. Otto, B. Vogel-Heuser, M. Zimmermann, and K. Stahl, "High-ratio planetary gearbox with ec gearing for robot applications," *International Journal of Intelligent Robotics and Applications*, pp. 1–11, 2024.

[5] D. Buleandra, A. Băneasă, and R. Donca, "3d printed harmonic drive for legged mobile robots," in *International Conference on Robotics in Alpe-Adria Danube Region*, pp. 597–605, Springer, 2024.

[6] K. Lee, S. Hong, and J.-H. Oh, "Development of a lightweight and high-efficiency compact cycloidal reducer for legged robots," *International Journal of Precision Engineering and Manufacturing*, vol. 21, no. 3, pp. 415–425, 2020.

[7] L. X. Xu, B. K. Chen, and C. Y. Li, "Dynamic modelling and contact analysis of bearing-cycloid-pinwheel transmission mechanisms used in joint rotate vector reducers," *Mechanism and Machine Theory*, vol. 137, pp. 432–458, 2019.

[8] H. Satake and N. Takesue, "Comparison of characteristics of cycloidal gear reducer using metal, plastic and 3d printed parts," in *2024 IEEE/SICE International Symposium on System Integration (SII)*, pp. 1531–1536, IEEE, 2024.

[9] C. Wang, "A study of the dynamic transmission efficiency of the cycloid pin gear pair under dynamic characteristic analysis," *Journal of Vibration and Control*, p. 10775463241296579, 2024.

[10] C. Barsomian, N. Eswaran, M. Pesenti, M. Gandolla, F. Braghin, E. Carpanzano, and L. Roveda, "Dynamic characterization and control of a back-support exoskeleton 3d-printed cycloidal actuator," *CIRP Annals*, vol. 73, no. 1, pp. 29–32, 2024.

[11] L. Maccioni, F. Concli, and M. Blagojevic, "A new three-stage gearbox concept for high reduction ratios: Use of a nested-cycloidal architecture to increase the power density," *Mechanism and Machine Theory*, vol. 181, p. 105203, 2023.

[12] X. Li, Y. Li, W. Niu, and R. Guo, "Design and analysis of a novel actuator with a double-roller gear drive," in *Actuators*, vol. 12, p. 292, MDPI, 2023.

[13] L. X. Xu, J. L. Zhong, Y. Li, and L. Chang, "Design and dynamic transmission error analysis of a new type of cycloidal-pin reducer with a rotatable output-pin mechanism," *Mechanism and Machine Theory*, vol. 181, p. 105218, 2023.

[14] L.-C. Tung and Y. J. Chan, "A time-variant dynamic model for compound epicyclic–cycloidal reducers," *Mechanism and Machine Theory*, vol. 179, p. 105095, 2023.

[15] M. Blagojevic, N. Marjanovic, Z. Djordjevic, B. Stojanovic, and A. Disic, "A new design of a two-stage cycloidal speed reducer," *Journal of Mechanical Design*, vol. 133, 2011.

[16] W.-S. Lin, Y.-P. Shih, and J.-J. Lee, "Design of a two-stage cycloidal gear reducer with tooth modifications," *Mechanism and Machine Theory*, vol. 79, pp. 184–197, 2014.

[17] R. Bezzini, G. Bassani, C. Alberto Avizzano, and A. Filippeschi, "Design of a novel flat cycloidal-planetary series reducer and experimental assessment for assistive exoskeletons actuation-cyplo," *IEEE Access*, vol. 13, pp. 202619–202631, 2025.

[18] T.-C. Lin, M. Schabacker, Y.-L. Ho, T.-C. Kuo, and D.-M. Tsay, "Geometric design and dynamic analysis of a compact cam reducer," *Machines*, vol. 10, no. 10, p. 955, 2022.

[19] H. Yang, Y. Li, J. Huang, X. Li, and L. Sun, "Theoretical analysis and performance prediction of a nn-type precision cycloidal reducer," *Forschung im Ingenieurwesen*, vol. 88, no. 1, p. 44, 2024.

[20] R. Bezzini, G. Bassani, C. A. Avizzano, and A. Filippeschi, "Design and experimental evaluation of multiple 3d-printed reduction gearboxes for wearable exoskeletons," *Robotics*, vol. 13, no. 11, p. 168, 2024.

[21] W. Roozing and G. Roozing, "3d-printable low-reduction cycloidal gearing for robotics," in *2022 IEEE/RSJ International Conference on Intelligent Robots and Systems (IROS)*, pp. 1929–1935, 2022.

[22] A. Kakogawa, Y. Mori, T. Fukasawa, N. Kurimoto, S. Tokunaga, T. Tokuda, A. Yamamoto, and S. Kawamura, "A highly backdrivable robotic arm using low friction and high accuracy cycloidal geared motors: Alfha," in *2022 IEEE/SICE International Symposium on System Integration (SII)*, pp. 428–433, IEEE, 2022.

[23] W. Roozing and G. Roozing, "Experimental comparison of pin-wheel and non-pinwheel designs of 3d-printed cycloidal gearing for robotics," in *2024 IEEE International Conference on Robotics and Automation (ICRA)*, pp. 7091–7098, IEEE, 2024.

[24] R. Bezzini, "Q-CYC Cycloidal Gearbox: Quadruple Disk Solution for Compact-Cam Cycloidal Gearboxes." `https://github.com/RicBez/Q-CYC-Cycloidal-Gearbox.git`, 2025. GitHub repository [Online, Available].

[25] A. Kapelevich and L. AKGears, "High gear ratio epicyclic drives analysis," *ratio*, vol. 3, no. 10, pp. 62–67, 2013.

[26] I. Buj-Corral and E. E. Zayas-Figueras, "Comparative study about dimensional accuracy and form errors of fff printed spur gears using pla and nylon," *Polymer Testing*, vol. 117, p. 107862, 2023.